

**NASA Technical Memorandum 82966**

(NASA-TM-82966) EVALUATION OF ELECTRODE  
SHAPE AND NONDESTRUCTIVE EVALUATION METHOD  
FOR WELDED SOLAR CELL INTERCONNECTS (NASA)  
14 p HC A02/MF A01

N83-10555

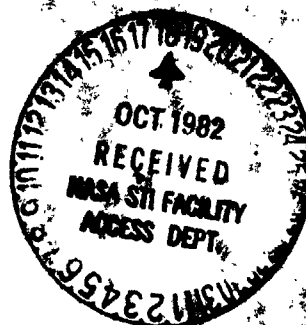
CSC 10A

Unclas

G3/44 35531

# Evaluation of Electrode Shape and Nondestructive Evaluation Method For Welded Solar Cell Interconnects

C. R. Baraona, S. J. Klima, T. J. Moore,  
W. E. Frey, and A. F. Forestieri  
*Lewis Research Center  
Cleveland, Ohio*



Prepared for the  
Sixteenth Photovoltaic Specialists Conference  
sponsored by the Institute of Electrical and Electronic Engineers  
San Diego, California, September 27-30, 1982

**NASA**

EVALUATION OF ELECTRODE SHAPE AND NONDESTRUCTIVE EVALUATION METHOD  
FOR WELDED SOLAR CELL INTERCONNECTS

C. R. Baraona, S. J. Klima, T. J. Moore  
W. E. Frey and A. F. Forestieri

National Aeronautics and Space Administration  
Lewis Research Center  
Cleveland, Ohio 44135

ABSTRACT

Resistance welds of solar cell interconnect tabs were evaluated. Both copper-silver and silver-silver welds were made with various heat inputs and weld durations. Parallel gap and annular gap weld electrode designs were used. The welds were analyzed by light microscope, electron microprobe and scanning laser acoustic microscope. These analyses showed the size and shape of the weld, the relationship between the acoustic micrographs, the visible electrode footprint, and the effect of electrode misalignment. The effect of weld heat input on weld microstructure was also shown.

INTRODUCTION

In space solar arrays, photovoltaic cells are interconnected in series-parallel strings by metal conductor tabs. These interconnects are usually soldered to the solar cell contact metallization at temperatures below 200°C. Resistance welding, proposed some time ago (1), is a higher temperature joining method that is an attractive alternative to soldering. Benefits of welded interconnects are significant. Welding allows increased array operating temperature and enables in-orbit annealing of radiation damage in the solar cells. Welded interconnects are expected to have greater resistance to thermal fatigue. Thus welding will extend the thermal cycling capability of space arrays and increase spacecraft lifetime. Welding will enable arrays to be hardened to space radiation through use of low atomic number materials like aluminum. Welding will also harden arrays to other hostile thermal environments such as those encountered in missions near the sun.

In spite of these benefits, welded arrays are not routinely used on United States spacecraft. Future acceptance of welding will be aided by mission need and by increased fundamental knowledge and experience. These latter categories include fundamental knowledge of weld microstructures and their relationship to weld conditions (2). In addition, experience with a nondestructive evaluation (NDE) technique to determine weld quality is also needed (3).

Resistance welding is usually accomplished by first pressing two electrodes against the interconnect tab forcing it against the cell contact. An electric current is then sent through the electrodes and into the interconnect where resistance heating occurs. The combination of heat and pressure causes the weld to form. Usually the electrodes are rectangular in cross section, parallel to each other and separated by a gap. Other geometries are also possible.

The American Welding Society (AWS) (4) defines three classes of weld metallurgy based on the physical state of the materials at the weld interface during coalescence. These terms are used in this report and are: fusion welding for liquid/liquid reaction, solid state welding for solid/solid reaction, eutectic brazing for liquid/solid reaction.

The purposes of the present work were to 1) determine microstructures of solar cell resistance welds and how they change with weld pulse energy and duration, 2) to verify the scanning laser acoustic microscope (SLAM) as a NDE method, and 3) to compare an annular gap electrode shape with the traditionally used parallel gap electrode.

PROCEDURE

Two types of molybdenum weld electrodes were used to make the welds. Figure 1a shows a pair of conventional parallel gap electrodes. The tips were rectangular in cross section measuring 0.65 mm by 1.25 mm on a side with a gap of 0.25 mm. Figure 1b shows a new annular gap electrode consisting of a center electrode 1.25 mm in diameter surrounded by an annular electrode. The outside diameter of the annulus was 2.0 mm and the inside diameter was 1.5 mm. The gap width was 0.13 mm.

The interconnect materials were either copper or silver foil 0.05 mm in thickness. Solar cells were 2 by 4 cm in size and had titanium, palladium, silver contacts with an aluminum back surface reflector. The cells were not encapsulated or attached to an array substrate or blanket material such as Kapton or

## ORIGINAL PAGE IS OF POOR QUALITY

aluminum honeycomb. The electrode tips maintained a load of 9 to 36 newtons on the tab during the welding operation (Hughes Model MCW-550 Welder). Voltage settings used ranged from 0.6 to 1.0 volt and were applied for 50 to 100 msec. The three weld schedules used to investigate the microstructure were:

- low heat input for a long time
- moderate heat input for a moderate time
- high heat input for a short time

The welded sections of the cells were mounted in clear epoxy and polished using standard metallographic techniques. Selected samples were examined using a scanning electron microscope and an electron probe microanalyzer to obtain quantitative elemental distribution along continuous line traverses through the weld regions. (The electron probe analysis was performed by Frank M. Terepka and is gratefully acknowledged.) Additional details of the sample preparation and analysis are given in references (2) and (3).

The principle of operation of the SLAM (5) is shown in figure 2. Ultrasonic sound at a frequency of 100 MHz passes through a solar cell sample and induces a dynamic ripple in a reflective coverslip touching the cell. A scanning laser beam is reflected into a photodetector producing a signal for a black and white television picture. In a SLAM picture, the brightest regions represent areas of good sound transmission and thus good weld bonding

### RESULTS AND DISCUSSIONS

Results from light microscope, SLAM, and metallographic sectioning are shown in figures 3 and 4. These results show that SLAM can determine the size, shape, and location of parallel gap and annular gap welds accurately.

Figure 3a shows the embossed imprint of a parallel gap electrode on a copper interconnect tab. The imprint is incomplete because of minor misalignment of the rectangular electrode faces to the copper surface. Figure 3b is a SLAM acoustic micrograph of the same weld area. Comparison of the figures shows that the weld zone is displaced upward relative to the electrode imprint and extends beyond the electrodes. The SLAM shows that the size of the weld may be either the white area or the white plus the grey area. The actual size of the welded area was determined by tearing away the soft copper tab. The tab was easily removed everywhere it was not welded to the cell. The remaining welded tab area is shown in figure 3c. Comparison of figures 3b and 3c shows that the SLAM slightly over-estimates the area of the weld which is only the white area in figure 3b. Cross-section AA in figure 3b was taken through a dark spot on the acoustic picture and is shown in figure 3d. This photomicrograph shows that the dark spot on the acoustic picture corresponds to an unwelded region only 200

micrometers (8 mils) long.

Figure 4 shows a similar analysis of an annular gap weld. Figure 4a shows a complete electrode imprint. The SLAM acoustic picture in figure 4b shows welding under a major portion of the outer annular electrode indicating slight misalignment. The entire center electrode area is welded. Cross section AA shown in figure 4c confirms the location of the welded and unwelded areas.

Weld metallurgy classes were identified by metallography and microprobe chemical analysis and reference to copper-silver or silver-silicon phase diagrams.(6). Results are shown in figures 5,6,7, and 10 for parallel gap welds made with copper tabs and a range of weld conditions. Figures 8 and 9 show similar results for annular gap welds with silver interconnects. In a single weld joint, a combination of metallurgical classes were observed regardless of weld electrode design.

Figures 5 through 9 each shows a cross section of a portion of a weld and a microprobe trace with atomic concentration in weight percent as a function of distance across the weld zone. The solid state weld shown in figure 5 has a well defined boundary between the copper interconnects and the silver contact with little interdiffusion near the copper-silver boundary. Solid state welds are more likely where electrode pressure is high and weld heat input is low for a long time.

A eutectic braze is shown in figure 6. It has a less distinct boundary and a concentration profile with more intermixing of the atoms than the solid state weld. A low melting point silver-28 weight percent copper eutectic was the braze metal present at the interface. There was little if any interdiffusion between the silver and the silicon.

A fusion weld nugget of copper, silver, palladium alloy is shown in figure 7. Large voids of trapped air and cracking of the silicon are evident. The weight percent concentration from the microprobe trace and the irregular weld nugget-cell interface are characteristic of melting and alloying. The quantity of palladium was small and was omitted from the microprobe data for clarity. Fusion welds are more likely when weld heat input is high.

Figure 8 shows a silver-silver solid state weld. The microprobe trace shows no significant silver-silicon interdiffusion. In figure 9 a silver-silicon eutectic braze was produced by higher energy input than in figure 8. Figure 9 shows evidence that a silver-4.5 weight percent silicon eutectic has formed in addition to the silver to silver solid state weld.

As stated above, in a single weld joint a combination of metallurgical classes were observed. Figure 10 illustrates the variation

## ORIGINAL RECORDS OF POOR QUALITY

of weld types with weld condition (i.e. heat input and weld duration) for a parallel gap electrode. Figure 10 is an estimate of the "evolution" of a copper-silver weld based on cross sections of numerous parallel gap welds and is not intended to be quantitative. A copper-silver weld was selected because more metallurgical classes are possible. Estimates can also be made for silver to silver welds and for annular gap electrodes but with less certainty because fewer samples of these types were examined. The three categories of welds shown in figure 10 are: 1) Low heat for a long time results in a solid state weld under the electrodes with an unwelded area between the electrodes. 2) Medium heat for a medium time results in a solid state weld under the electrodes and a eutectic braze between the electrodes. 3) High heat for a short time results in a solid state weld and eutectic braze under the electrodes and a eutectic braze and fusion weld between the electrodes. In each case the weld types overlap. A continuum of footprints exists. Even lower heat inputs would result in no welding and higher heat inputs would result in "burned" welds (i.e. gross melting and/or overheating and cracking).

### CONCLUSIONS AND RECOMMENDATIONS

The SLAM is a useful NDE technique for individual welded cells. The usefulness of SLAM as an in-process NDE method depends on extension of the SLAM from individual unencapsulated cells to solar array like structures. Welded cells in a blanket material or mounted on a substrate may have the ultrasonic sound transmission blocked or scattered and the resolution of the SLAM would be reduced.

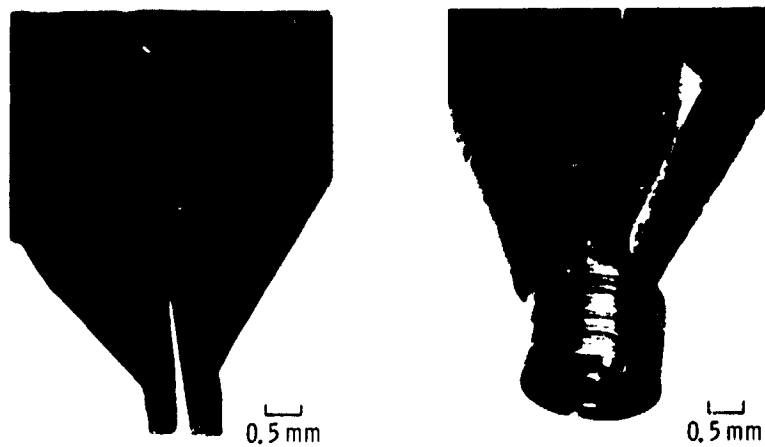
The metallurgical categories of resistance welds and their variation with weld condition

were determined by analysis of copper-silver and silver-silver welds made with parallel gap and annular gap electrodes. Further analysis of annular gap welds is necessary to reliably compare them to parallel gap welds. Additional work is also needed to relate weld metallurgy to performance in the space environment. For example weld pull strength and fatigue lifetime due to thermal cycling in orbit should be related to weld microstructure.

### REFERENCES

1. K. Reinhartz, and J. Capart, "Status of Welded Solar Cell Module Technology at ESRO," Proceedings of the Eighth IEEE Photovoltaic Specialists Conference, pp. 287-292, 1970.
2. Moore, T. J. Watson, G. K., and Baraona, C. R., "Microstructural Analysis of Solar Cell Welds," Proceedings of the Space Photovoltaic Research and Technology Conference, NASA Lewis Research Center, April 1982, to be published.
3. Klima, S. J., Frey, W. E., and Baraona, C. R.; Evaluation of Solar Cell Welds by Scanning Laser Acoustic Microscopy, Proceedings of the Space Photovoltaic Research and Technology Conference, NASA Lewis Research Center, April 1982, to be published.
4. "Welding Terms and Definitions," American Welding Society, A3.0-80, 1980.
5. L. W. Kessler, and D. E. Yuhas, "Acoustic Microscopy 1979," Proc. of the IEEE, vol. 67, no. 4, pp. 526-536, 1979.
6. M. Hansen, Constitution of Binary Alloys, New York: McGraw-Hill, 1958.

ORIGINAL PAGE  
BLACK AND WHITE PHOTOGRAPH



(a) CONVENTIONAL PARALLEL -  
GAP ELECTRODES.

(b) ANNULAR -GAP ELECTRODES.

Figure 1. - Resistance weld electrodes used for joining solar cell interconnects.

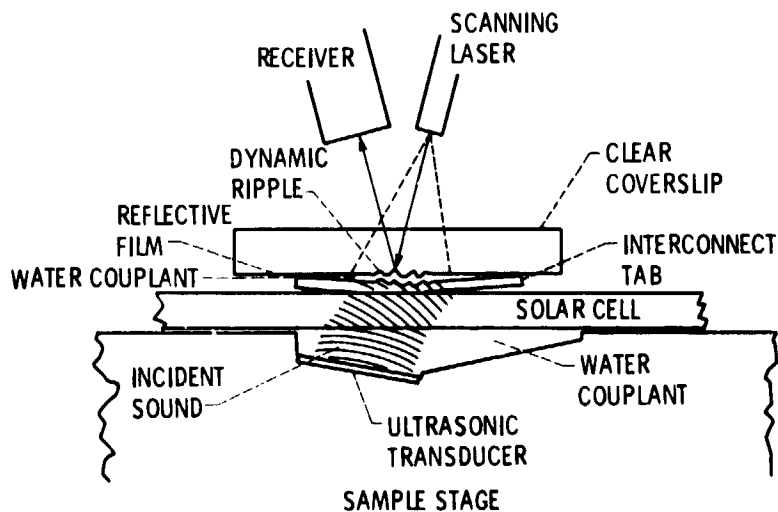
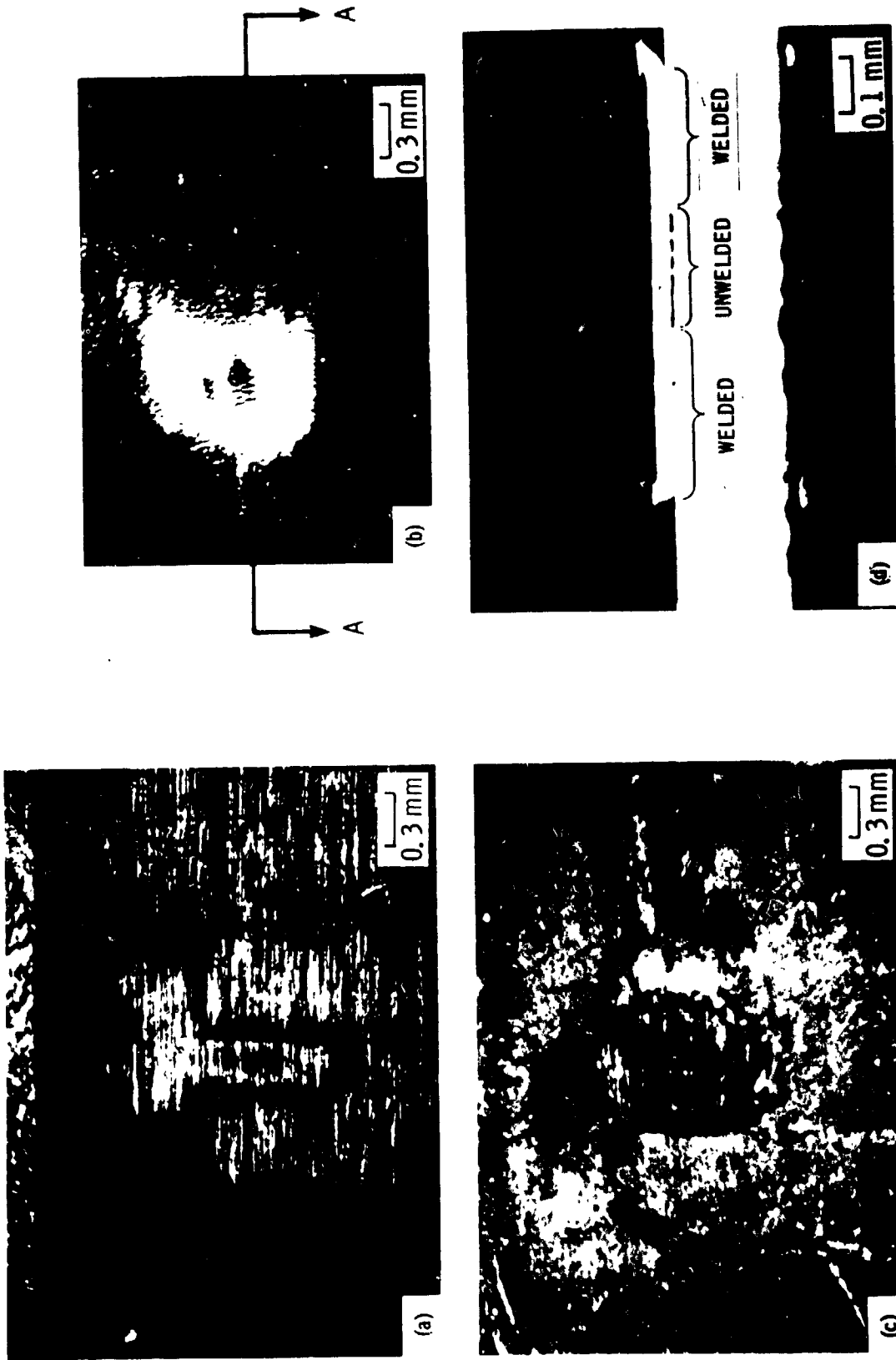


Figure 2. - Application of the scanning laser acoustic microscope for nondestructive evaluation of solar cell interconnect welds.

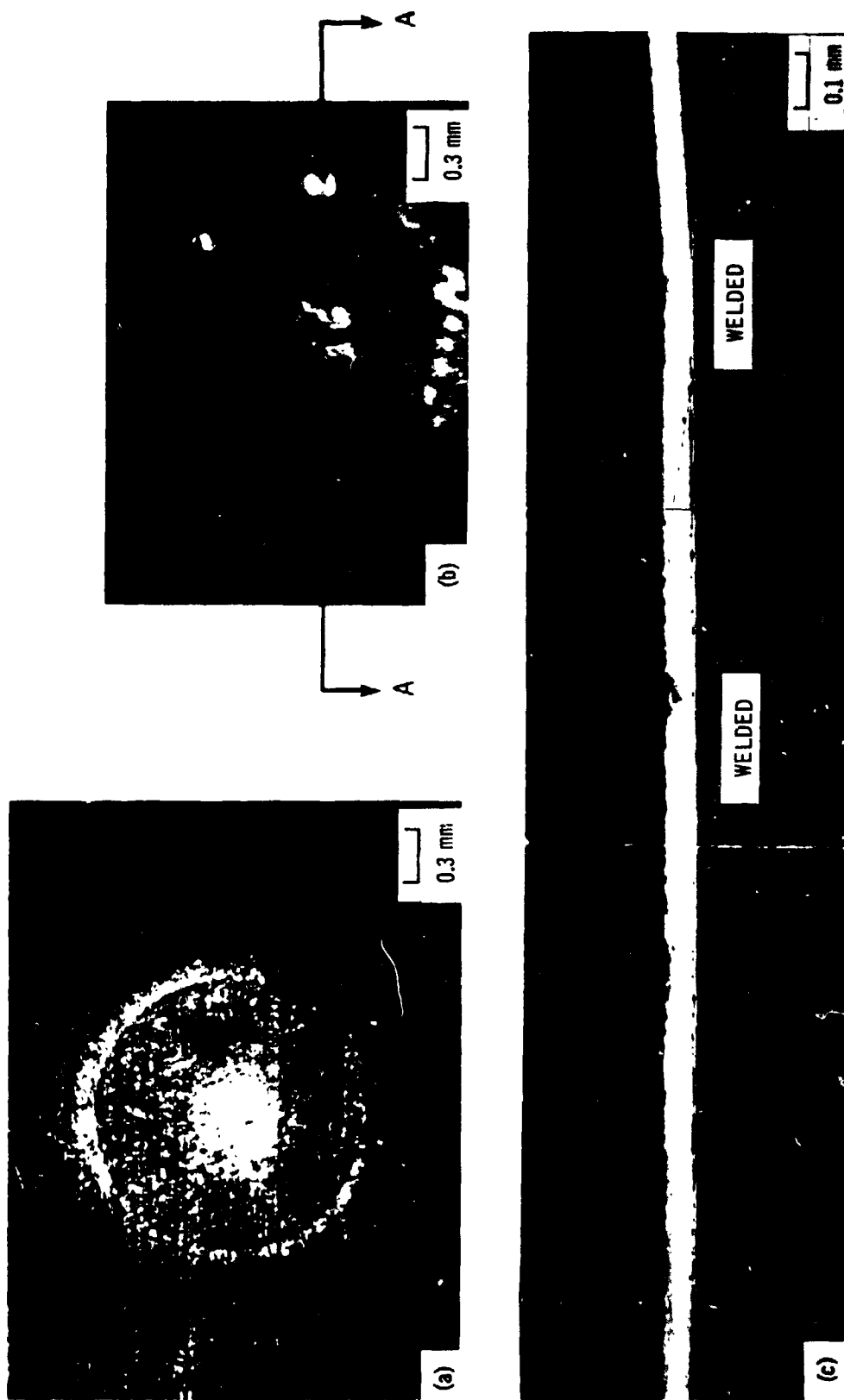
ORIGINAL PAGE  
BLACK AND WHITE PHOTOGRAPH



(a) Partial footprint on tab surface.  
(b) Acoustic micrograph of weld zone.  
(c) Nugget size revealed by removal of unwelded portion of tab.  
(d) Photomicrograph of cross-section A-A through middle of weld zone.

Figure 3. - Results of destructive and nondestructive analysis of Cu-Ag parallel-gap weld.

ORIGINAL PAGE  
BLACK AND WHITE PHOTOGRAPH



(a) Complete electrode imprint on tab surface.

(b) Acoustic micrograph of nearly complete weld.

(c) Photomicrograph of crosssection A-A through middle of weld zone.

Figure 4. - Results of destructive and nondestructive analysis of an Ag-Ag annular-gap weld.

MICROPROBE TRACE

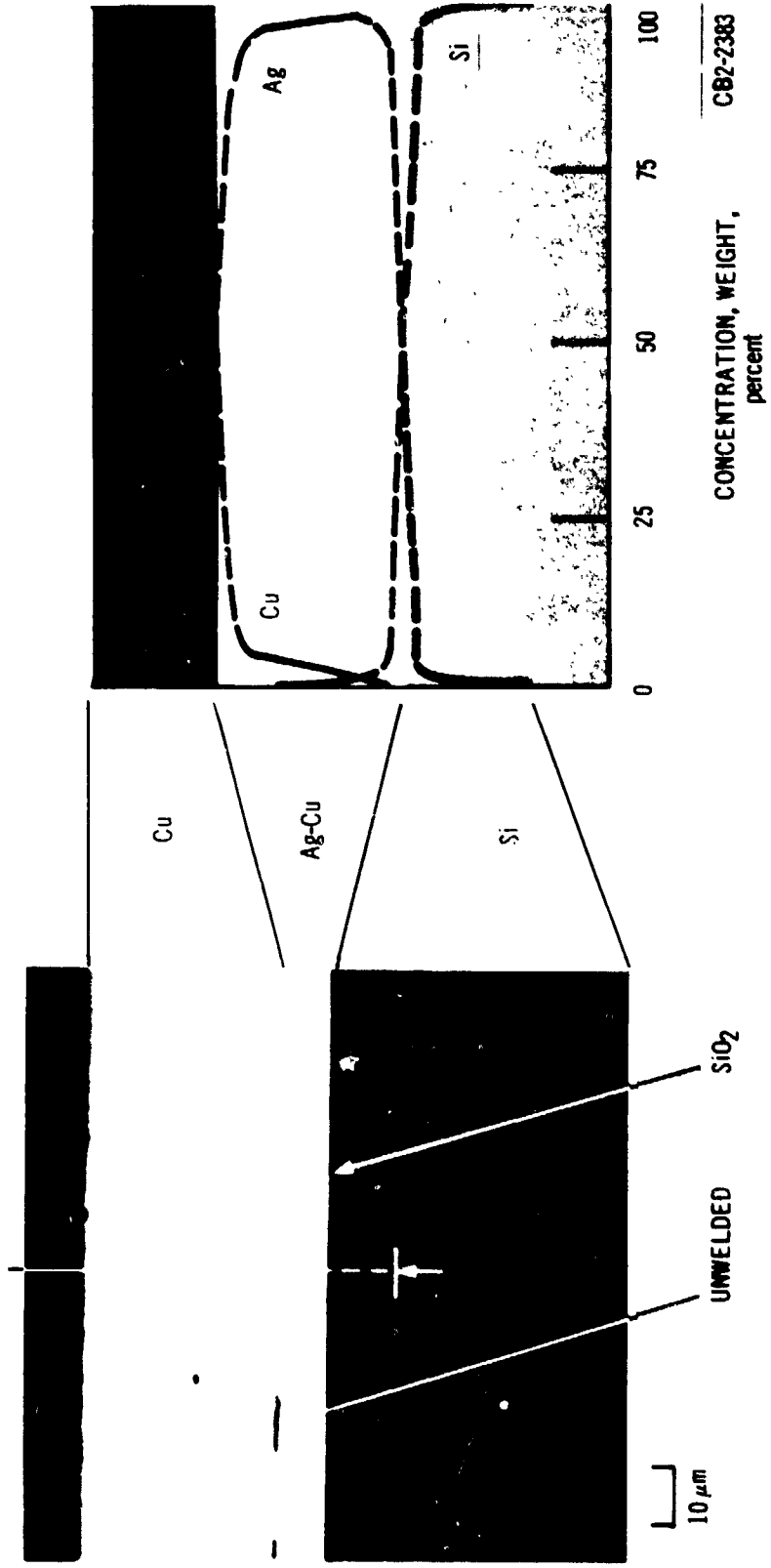


Figure 5. - Solid state weld at N contact area showing slight interdiffusion between Ag and Cu.



ORIGINAL PAGE  
BLACK AND WHITE PHOTOGRAPH

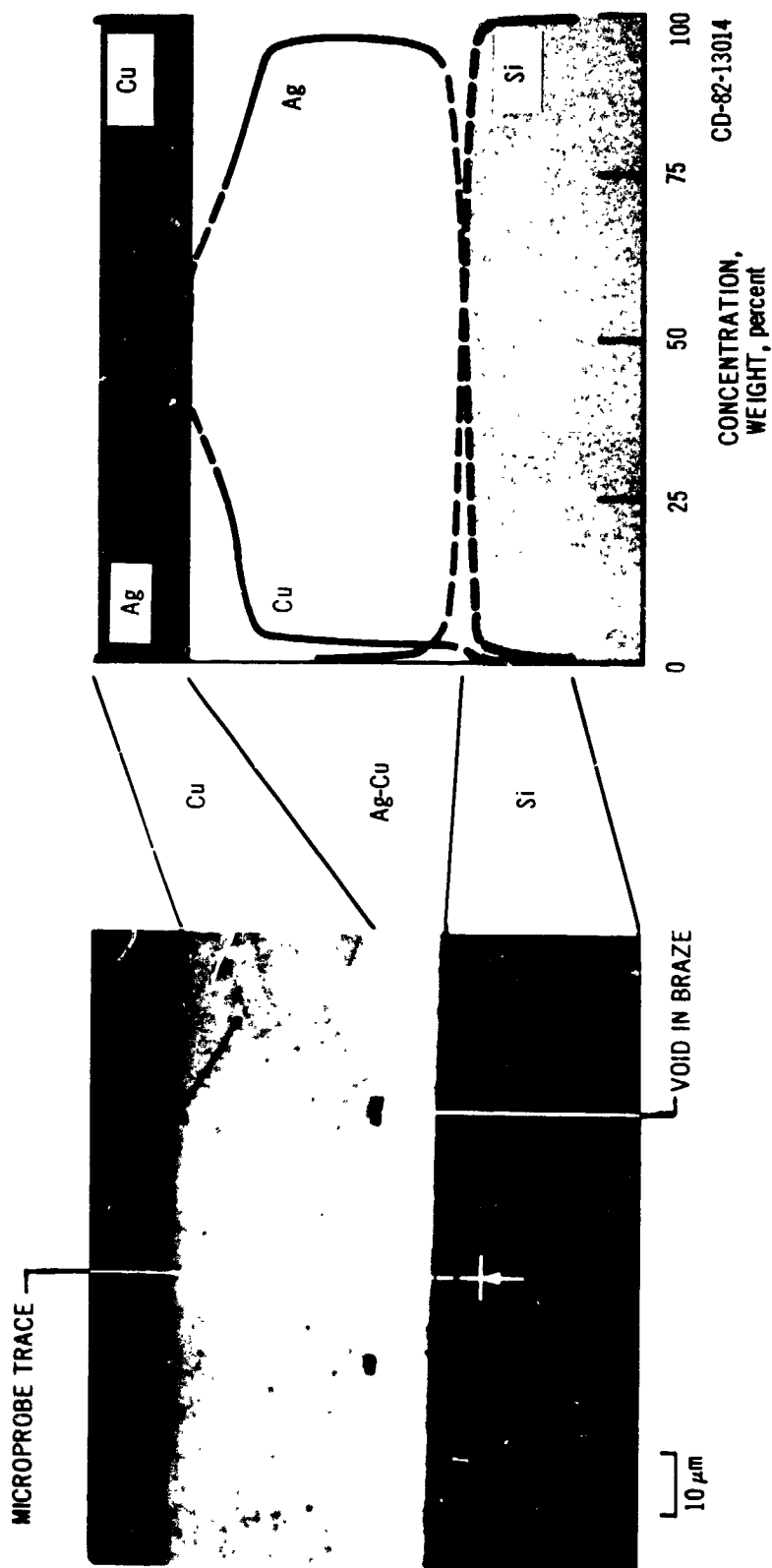


Figure 6. - Ag-Cu braze joint, approximately 2.5 μm wide, with small voids in the braze metal. Significant Ag-Cu alloying is shown at the braze in this P contact joint.

ORIGINAL PAGE  
BLACK AND WHITE PHOTOGRAPH

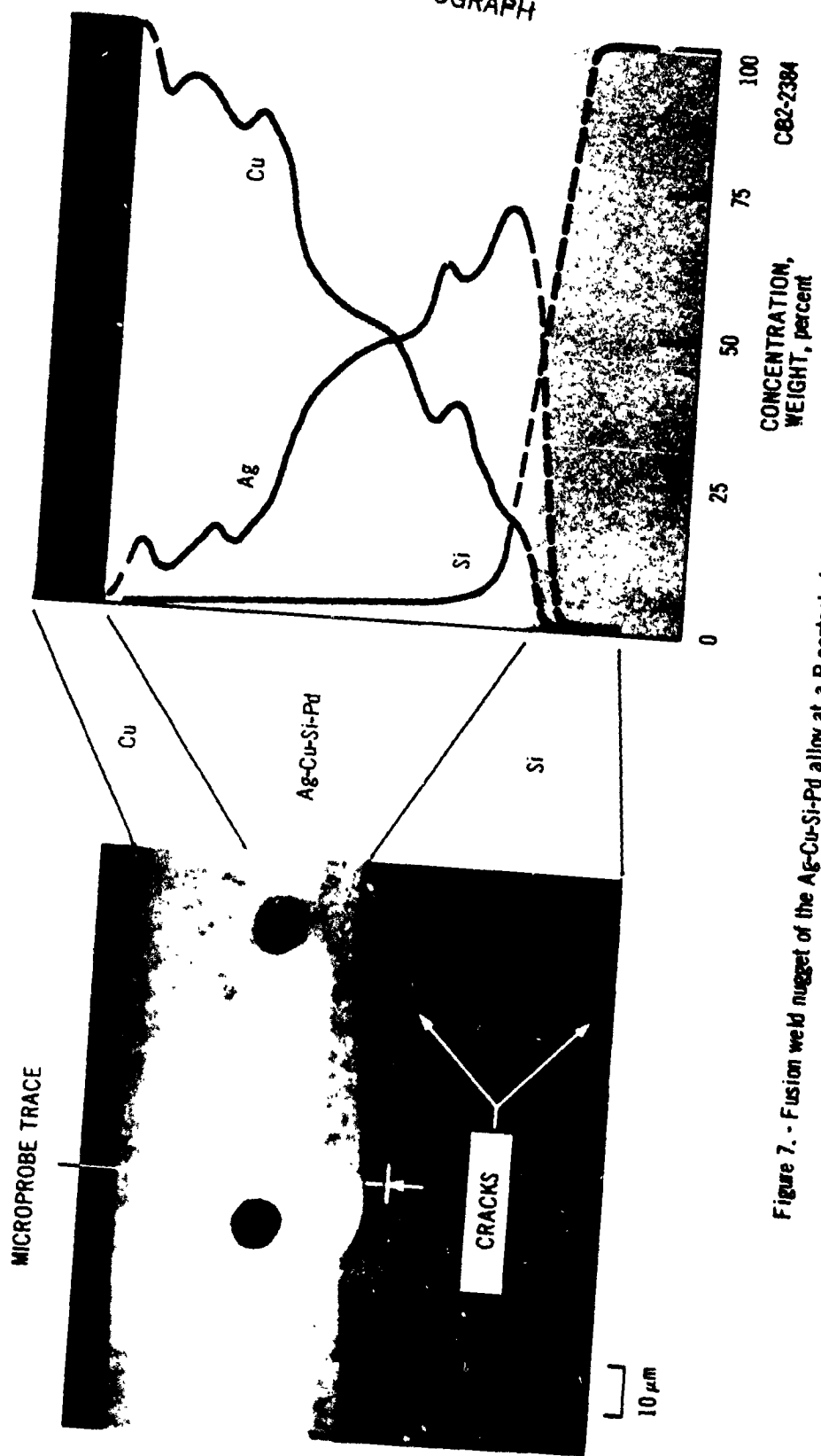


Figure 7. - Fusion weld nugget of the Ag-Cu-Si-Pd alloy at a P contact showing cracking in the Si cell.

ORIGINAL PAGE  
BLACK AND WHITE PHOTOGRAPH

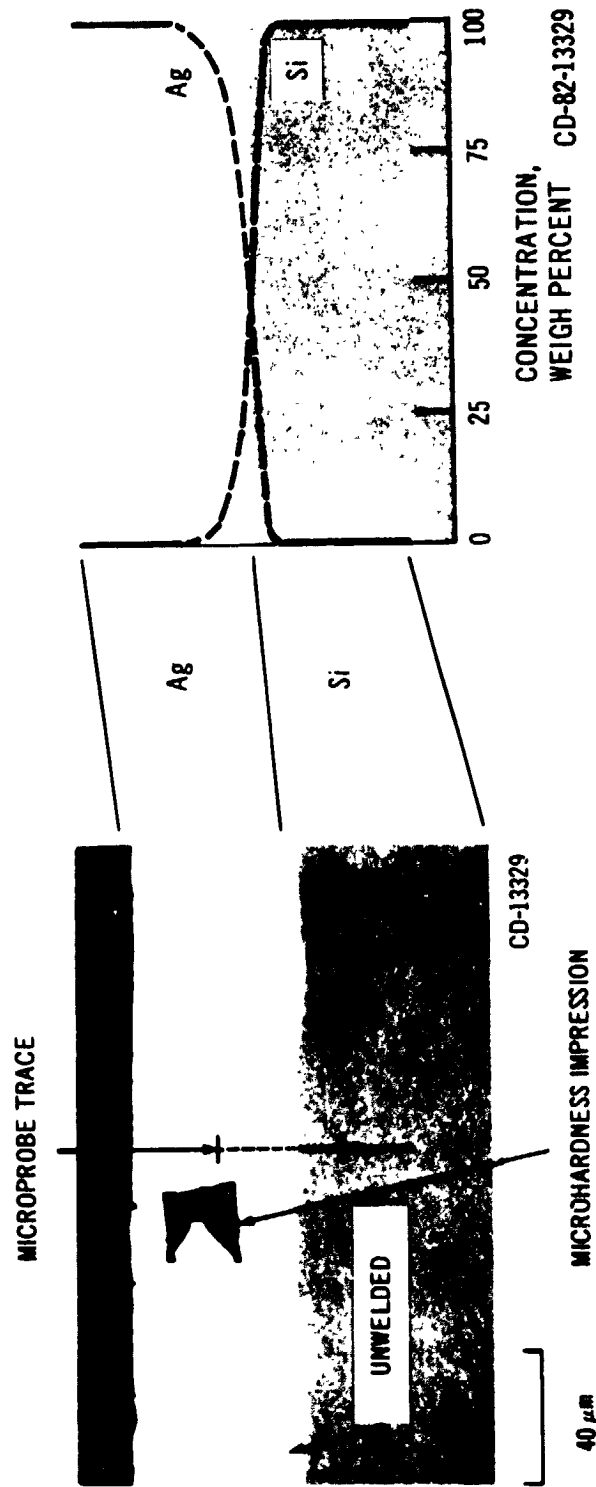


Figure 8. - Solid state Ag-Ag weld.

ORIGINAL PAGE  
BLACK AND WHITE PHOTOGRAPH

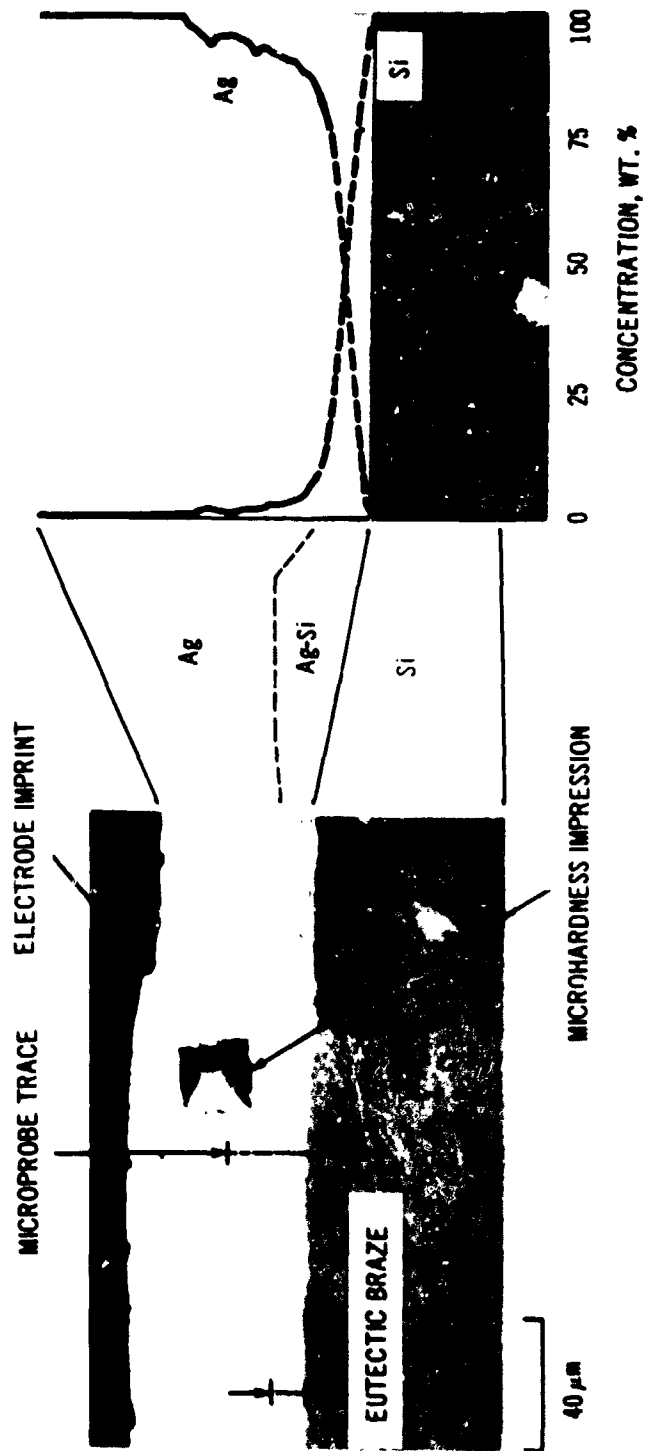


Figure 9. - Eutectic braze between Ag and Si.

CD-82-13328

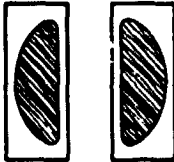
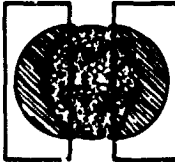
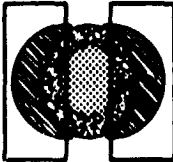
<b>WELD HEAT INPUT</b>	<b>LOW</b>	<b>MEDIUM</b>	<b>HIGH</b>
<b>WELD DURATION</b>	<b>LONG</b>	<b>MEDIUM</b>	<b>SHORT</b>
<b>FOOTPRINT (TOP VIEW)</b>			
<b>WELD TYPES</b>	<b>SOLID STATE</b>	<b>SOLID STATE AND EUTECTIC BRAZE</b>	<b>SOLID STATE EUTECTIC BRAZE AND FUSION NUGGET</b>

Figure 10. - Weld microstructure vs. weld condition for Ag-Cu joint with rectangular parallel gap electrodes.